GENE EXPRESSION ANALYSIS AND HEPATOPROTECTIVE ACTIVITY OF METFORMIN-LOADED CHITOSAN NANOPARTICLES AGAINST METHOTREXATE-INDUCED LIVER TOXICITY *IN VIVO*

N. Shamim[1], M. A. Rasheed[1]*, M. O. Omer[1] and W. Shehzad[2]

[1]Department of Pharmacology and Toxicology, University of Veterinary and Animal Sciences, Lahore
[2]Institute of Biochemistry and Biotechnology, University of Veterinary and Animal Sciences, Lahore
Corresponding Author's Email: dr_aadil@uvas.edu.pk

ABSTRACT

The adverse hepatotoxic effect is a great barrier for both drug development and pharmacotherapy because of its complex pathogenesis and unpredictable outcome. This research aimed to explore the hepatic toxicity and gene expression studies after the oral methotrexate administration in Wistar rats and the hepatoprotective efficacy of the metformin-loaded chitosan nanoparticles system. The nanoparticles (NPs) were synthesized by means of the ionic gelation technique with the use of the following instrumental approaches: Fourier Transform Infrared Spectroscopy, Scanning Electron Microscopy, polydispersity index, size, zeta potential analysis, drug entrapment efficiency, and *in vitro* drug release test. Metformin-loaded chitosan NPs exhibited a distinctive spectral peak of 3447 cm^{-1}, spherical shape, low PDI = 0.30, size of 213 nm, zeta potential of +28.1 mV, and drug entrapment efficiency of 97.34%. A total of 48 male Wistar albino rats (3–4 months old; 220 ± 25 g) were randomly allocated into eight groups (n = 6 per group) under a Completely Randomized Design (CRD) for hepatotoxicity evaluation based on biochemical, histopathological, and gene expression studies. The methotrexate treatment (Group B) caused a severe hepatotoxic and hematological effect with the increased ALT, AST, ALP, total bilirubin serum concentrations and decreased total protein, albumin, TLC, hemoglobin, RBC, HCT, and platelets count compared to the normal control ($p \leq 0.001$). These alterations were markedly attenuated by metformin-loaded chitosan nanoparticles (Met-CSNPs), particularly at 75 mg/kg/day (Group H), which produced the most favorable biochemical and hematological profile among the nanoparticle-treated groups. Histopathological examination revealed Met-CSNP treatment progressively reduced hepatic injury, with the 75 mg/kg/day dose showing the greatest tissue preservation and no detectable fibrosis. Gene-expression analysis demonstrated significant suppression of hepatic *TIMP1* and *TGF-β* expression relative to the MTX toxic-control group, with a graded dose-response across the 25, 50, and 75 mg/kg/day Met-CSNP doses. The 75 mg/kg/day formulation produced the greatest reduction in *TGF-β* expression (0.51-fold relative to the normal control) and the strongest overall suppression of *TIMP1* among the nanoparticle-treated groups. Overall, Met-CSNPs demonstrated dose-dependent hepatoprotective and anti-fibro genic effects against MTX-induced hepatic injury, with the 75 mg/kg/day formulation showing the most pronounced protective response.

Keywords: Chitosan nanoparticles, Nanoparticle drug delivery, Hepatic protection, Toxicity attenuation.

Received May 19, 2026 Published Online October 19, 2026 https://doi.org/10.36899/JAPS.2027.1.0004

INTRODUCTION

Drug-induced liver damage (DILI) is becoming a significant concern for general health. DILI commonly results in a broad range of symptoms, from mild non-specific symptoms, such as acute hepatitis, chronic hepatitis, and cholestasis, to acute conditions, i.e., liver failure (Kozielewicz *et al*., 2025). DILI is one of the most significant causes of liver dysfunction. Numerous prescription medications, herbal remedies, and nutritional supplements have been reported to cause DILI (Ozturk *et al*., 2024). Biological agents, traditional Chinese medicine (TCM), natural medicine (NM), health care products (HP), dietary supplements (DS), their metabolites, and excipients are mostly prescribed against DILI. Acetaminophen caused drug-induced liver injury (DILI) is well documented following both acute and chronic exposure (Ezhilarasan, 2021). Additionally, drugs such as statins and anti-tuberculosis medicines can induce minor and temporary aberrations in liver-related parameters. Such aberrations may return to baseline values if regular treatment is maintained. These aberrations indicate moderate liver damage that resolves on its own (Ezhilarasan, 2021; Naqvi *et al*., 2015).

Methotrexate (MTX), formerly referred to as amethopterin, is categorized as a Class III compound under the Biopharmaceutical Classification System (BCS). MTX is commonly prescribed for the management of inflammatory and

autoimmune diseases such as rheumatoid arthritis (RA), idiopathic arthritis, vasculitis, Crohn's disease, myasthenia gravis, multiple sclerosis, and sarcoidosis as well as dermatological disorders such as psoriasis and atopic dermatitis (Bedoui *et al*., 2019; Pivovarov and Zipursky, 2019). MTX controls the equilibrium between tissue breakdown and tissue regeneration that is important for RA management. The usefulness of methotrexate (MTX) is constrained due to its ability to cause hepatotoxicity that is one of the most prominent side effects of the drug. Methotrexate (MTX) induces hepatotoxicity by inhibiting DNA and RNA synthesis, resulting in cell cycle arrest and subsequent cellular injury (Pivovarov and Zipursky, 2019). Additionally, long-term MTX administration can cause serious problems such as fibrosis, cirrhosis, and portal hypertension (Koźmiński *et al*., 2020).

Metformin is regarded as the first-line treatment in type 2 diabetes mellitus (DM) and offers multiple advantages over other currently available oral antidiabetic drugs (Rojas and Gomes, 2013). It can exert a direct vascular anti-inflammatory effect by inhibiting nuclear factor Kappa B (NF-κB) and interleukin (IL)-1β-induced proinflammatory cytokines (Gujytė *et al*., 2026). Metformin exerts additional hepatoprotective effects by upregulating heme oxygenase-1 (HO-1), thereby attenuating oxidative stress-induced apoptosis in primary rat hepatocytes. Nanotechnology has been widely applied in the field of medicine, particularly in the development of nanomedicine (Bayda *et al*., 2019). Similarly, in medical treatment, nanoparticle-based oral medications could be helpful in DILI treatment. Biodegradable polymers such as chitosan have demonstrated well-ordered drug release and increased pharmacological interactions with target cells (Naskar *et al*., 2019). The novelty of the present study lies in the development of a metformin-loaded chitosan nanoparticle formulation and its comprehensive evaluation against methotrexate-induced hepatotoxicity using biochemical, histopathological, and fibrosis-associated gene expression analyses (Mathane *et al*., 2025). Unlike previous studies that primarily focused on either the pharmacological effects of metformin or the physicochemical characteristics of chitosan nanoparticles, the present work integrates both approaches to investigate whether nanoparticle-mediated delivery enhances the hepatoprotective efficacy of metformin in a preclinical model. This integrated therapeutic strategy provides new evidence supporting nanotechnology-assisted metformin delivery as a promising intervention for drug-induced liver injury (Al-Bhadly and Mnati, 2025).

Histopathological evaluation is widely regarded as the reference standard for assessing methotrexate-induced hepatic injury, as it provides direct visualization of structural and cellular alterations within liver tissue. Repeated administration of methotrexate progressively impairs hepatic architecture, leading to histopathological abnormalities such as hepatocellular degeneration, inflammatory cell infiltration, sinusoidal dilatation, oxidative stress-associated necrosis, and fibrosis. All of the changes mentioned above represent the aggregate effects of methotrexate toxicity on the liver (Brennan *et al*., 2022).

While serum biochemical tests can serve as an indirect tool to identify any damage done to the liver, histopathological tests can be used as a direct method to assess liver architecture and tissue damage. Thus, histopathological examination is one of the key endpoints in assessing the extent of liver damage and treatment of hepatoprotective agents (Ezhilarasan *et al*., 2025). Fibrosis is a complicated disease process involving the activation of multiple profibrogenic signaling pathways, with *TGF-β* being the key mediator of the activation of hepatic stellate cells and ECM synthesis. *TIMP1* further stimulates fibrosis through the inhibition of matrix metalloproteinases, resulting in reduced ECM degradation and collagen accumulation in the liver tissue (Gardner and Ghorpade, 2003). The consistent overexpression of *TGF-β* and *TIMP1* has been closely linked with the occurrence and progression of methotrexate-induced liver fibrosis and other liver diseases (Meng *et al*., 2016). Consequently, the evaluation of the expression of these genes involved in fibrosis helps to understand the molecular basis of liver damage and thus constitutes an effective method to measure the antifibrotic effectiveness of new drugs (Zhang *et al*., 2021).

This study aimed to formulate metformin-loaded chitosan nanoparticles (Met-CSNPs) and assess their protective effects against methotrexate-induced hepatotoxicity after oral administration. Hepatic protection was evaluated by comparing hematological parameters, liver function biomarkers and histopathology of liver tissues among the experimental groups. To further elucidate the mechanism of action, molecular investigations were performed by examining changes in fibrosis-associated gene expression.

MATERIALS AND METHODS

Ethical Considerations: The study was conducted at the Postgraduate Laboratory following approval from the Ethics Review Committee of the University of Veterinary and Animal Sciences, Pakistan. Ethical approval was granted under Ethical Certificate No. DR/381, dated 18 August 2023. All experimental procedures involving rats were conducted in accordance with institutional guidelines for rat handling, care, experimentation, and humane euthanasia. The experimental procedures and reporting were conducted with consideration of the principles outlined in the ARRIVE 2.0 guidelines for reporting rat research.

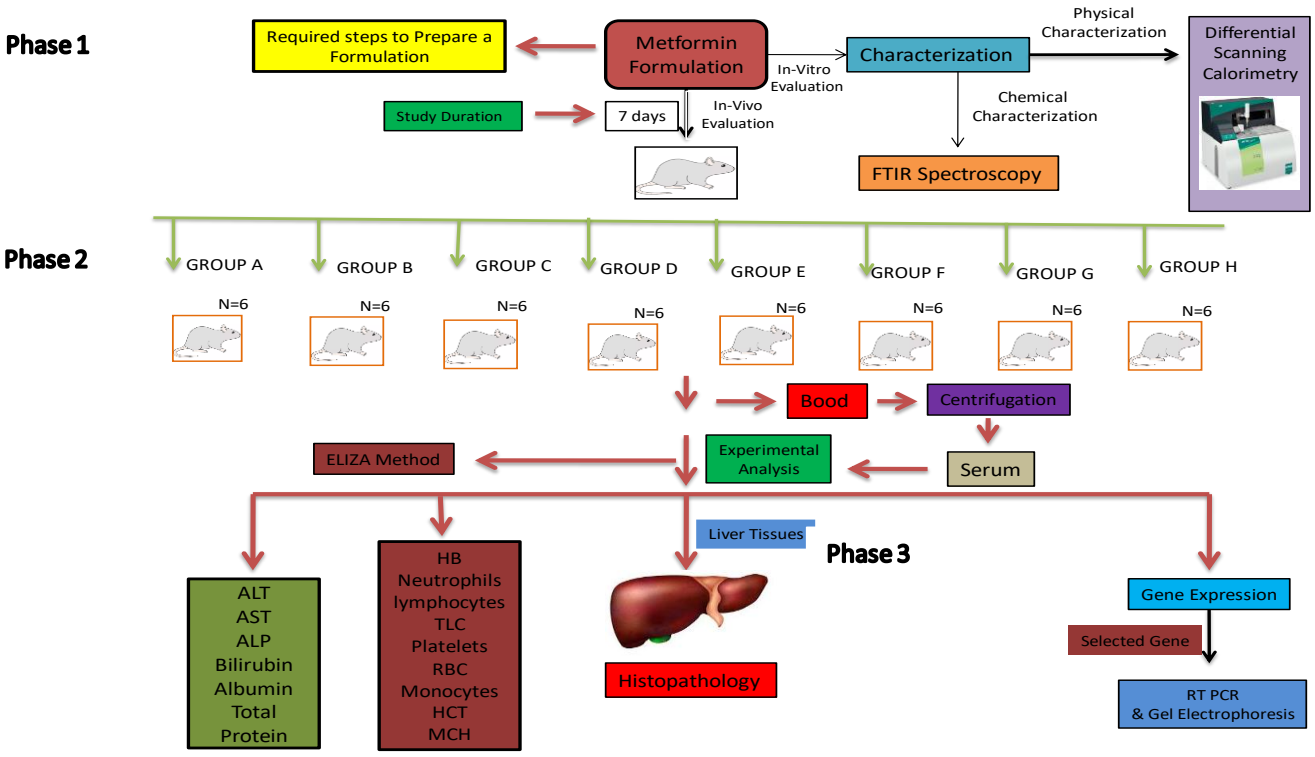

Figure 1. Treatment protocol and experimental grouping for the gene-expression and hepatoprotective evaluation of Met-CSNPs against methotrexate-induced liver toxicity.

Chemicals and Drugs: All chemicals and reagents were obtained from commercial suppliers and used as received. Methotrexate (≥98% purity; Sigma-Aldrich, USA; Cat. No. M8407), metformin hydrochloride (Sigma-Aldrich; Cat. No. D150959), chitosan (75–85% deacetylated; Sigma-Aldrich; Cat. No. 448869), and sodium tripolyphosphate (technical grade; Sigma-Aldrich; Cat. No. 238503) were used for nanoparticle preparation. Solvents included glacial acetic acid (≥99.8%; Merck, Germany; Cat. No. 100063), ethanol (lab grade, 96%; Merck; Cat. No. 100983), and formaldehyde solution (37%; Merck; Cat. No. 104003). For molecular biology analyses, RNA was extracted using TRIzol™ Reagent (Thermo Fisher Scientific, USA; Cat. No. 15596026), cDNA was synthesized with the RevertAid First Strand cDNA Synthesis Kit (Thermo Scientific; Cat. No. K1622), and quantitative PCR was performed using PowerUp™ SYBR™ Green Master Mix (Thermo Fisher Scientific; Cat. No. A25742).

Preparation of Metformin-Loaded Chitosan Nanoparticles (Met-CSNPs): Metformin hydrochloride (10 mg) was dissolved at a concentration of 1 mg/mL in 10 mL of an ethanol: water mixture (30:70, v/v). Separately, chitosan was dissolved at a concentration of 0.2% w/v in 1% v/v acetic acid. The metformin solution was gradually added to the chitosan solution and continuously stirred for 30 min at room temperature to allow equilibration. The pH of the resulting solution was adjusted to 5.0 using 1 M sodium hydroxide (NaOH). Sodium tripolyphosphate (TPP) solution (1 mg/mL, w/v) was then added dropwise to the metformin-containing chitosan solution under continuous stirring at 700 rpm. The TPP-to-chitosan mass ratio was maintained at 1:5 (w/w). The mixture was further stirred at 700 rpm for an additional 30 min at room temperature to facilitate ionic cross-linking and formation of Met-CSNPs. The resulting nanoparticle dispersion was subjected to ultracentrifugation at 72,002 × g for 30 min. The supernatant containing the free, non-entrapped metformin was carefully collected for subsequent determination of drug entrapment efficiency, whereas the nanoparticle pellet was recovered for further characterization and experimental use (Awchee *et al*., 2026).

Characterization of Nanoparticles: The prepared nanoparticles were characterized for their physicochemical properties, including physical stability, chemical characteristics, morphology, surface charge, polydispersity, practical yield, drug entrapment efficiency, and *in vitro* drug-release behavior.

Physical Stability: Physical stability was assessed at baseline and predetermined intervals by evaluating visual appearance, particle size, PDI, and zeta potential. The physical stability of the Met-CSNPs was evaluated over a 90-days

period under refrigerated conditions (4 ± 2°C) and ambient conditions (25 ± 2°C). Changes in the physical characteristics of the formulation were monitored during the storage period.

Fourier-Transform Infrared Spectroscopy: FTIR spectroscopy was used to characterize the chemical structure of the nanoparticle formulation and assess possible interactions between metformin and the chitosan-based formulation. FTIR spectra were recorded over the range of 4000–400 cm^{-1}. Characteristic absorption bands were evaluated to identify functional groups and assess the chemical characteristics of the formulation. The reported characteristic bands included approximately 3447 cm^{-1} and 1639 cm^{-1}, corresponding to functional groups associated with $–NH_2$ and –OH groups and related hydrogen-bonding/amide characteristics (Guadarrama-Escobar *et al*., 2023).

Scanning Electron Microscopy: The surface morphology and structural characteristics of the nanoparticles were examined using scanning electron microscopy (SEM) with an FEI Nova 450 Nano SEM. Nanoparticle samples were prepared for SEM examination and imaged at approximately 15,000–35,000× magnification using an accelerating voltage of 20–30 kV. Representative micrographs were obtained to evaluate nanoparticle morphology and surface characteristics (Santhosh Kumar *et al*., 2017).

Particle-Size Distribution, Polydispersity Index and Zeta Potential: Evaluation of nanoparticle dispersion was done for particle size distribution, polydispersity index (PDI), and zeta potential by electrophoretic/ light scattering technique. The sample was properly diluted with distilled water prior to its analysis. The PDI was found to be approximately 0.28-0.30, which is an indication of particle size distribution in the formulation. Zeta potential determination was done in the presence of electric field strength of 15.2V/cm.

Drug entrapment efficiency: It was evaluated by the isolation of free-metformin that is not entrapped in the nanoparticle formulation by centrifuging. The concentration of the free metformin in the isolated supernatant was determined by UV spectrophotometer with wavelength of 277nm. Entrapment efficiency was calculated using:

Entrapment efficiency (%) = [(Total amount of drug − Amount of free drug) / Total amount of drug] × 100

The resulting value represented the proportion of metformin successfully associated with or entrapped within the chitosan nanoparticle formulation (Singh *et al*., 2023).

***In Vitro* Drug-Release Study:** The *in vitro* metformin release from chitosan nanoparticles was carried out by using the dialysis membrane technique. The nanoparticles were suspended in 2 mL of 0.1 N HCl and placed in the dialysis membrane having a molecular weight cut-off value of 12,400 Da (Sigma-Aldrich, USA). This membrane was tightly sealed and placed in 100 mL of 0.1 N HCl in a 250 mL beaker. The release medium was maintained at 37°C under continuous magnetic stirring. At predetermined time intervals, aliquots of the release medium were withdrawn and replaced with an equivalent volume of fresh release medium to maintain the volume and release conditions. The amount of metformin released into the medium was quantified by UV spectrophotometry at 277 nm, and the cumulative drug-release profile was determined over the study period (Mast *et al*., 2021).

Experimental protocol: A total of 48 male Wistar albino rats, aged 3–4 months and weighing approximately 220 ± 25 g, were included in the experimental study. The sample size consisted of six rats per group, giving a total of eight experimental groups (n = 6/group; total n = 48). The sample size was adopted according to an experimental protocol involving a comparable methotrexate-induced hepatotoxicity model (Hafez and Elbassuoni, 2022). The rats were housed under controlled laboratory conditions at approximately 25 ± 2°C, with a 12-h light/12-h dark cycle and free access to drinking water. Rats underwent a two-week acclimatization period before commencement of the experimental treatment.
Experimental Design and Group Allocation: Following acclimatization, the rats were randomly allocated into eight experimental groups under Completely Randomized Design (CRD), using computer-generated randomization sequence, with six rats in each group. Individual rat represented the biological replicates. Methotrexate was administered at the same dose in Groups B–H where specified in the experimental protocol. The metformin-loaded nanoparticle doses were consistently expressed as 25, 50, and 75 mg/kg/day for Groups F, G, and H, respectively.

Treatment Administration and Experimental Duration: The experimental treatment protocol was followed as per the treatment schedule; methotrexate was given orally on a weekly basis while other respective protective/treatment agents were given daily as per requirement. The experimental period was 56 days. Longitudinal hematological and biochemical measures were taken on Days 1, 14, 28, 42, and 56. Day 1 was the baseline/pre-treatment measure, while the rest of the measurements were the response to the experimentally given treatment.

The experimental groups were as follows:

Group	Treatment
A – Negative control	Normal saline only
B – Positive/toxic control	Methotrexate 25 mg/kg, orally, once weekly
C – Blank nanoparticle control	Blank/simple chitosan nanoparticles
D – Silymarin treatment	Methotrexate 25 mg/kg orally once weekly + silymarin 100 mg/kg/day orally
E – Free metformin treatment	Methotrexate 25 mg/kg orally once weekly + metformin 250 mg/kg/day orally
F – Low-dose nanoparticle treatment	Methotrexate 25 mg/kg orally once weekly + metformin-loaded chitosan nanoparticles 25 mg/kg/day orally
G – Intermediate-dose nanoparticle treatment	Methotrexate 25 mg/kg orally once weekly + metformin-loaded chitosan nanoparticles 50 mg/kg/day orally
H – High-dose nanoparticle treatment	Methotrexate 25 mg/kg orally once weekly + metformin-loaded chitosan nanoparticles 75 mg/kg/day orally

Blood Sampling and Hematological Analysis: Baseline blood sample was drawn prior to the administration of methotrexate or treatment protocol. Thereafter, methotrexate and treatment protocol were started as per experimental schedule. 1.5 mL blood samples were drawn at Days 1, 14, 28, 42, and 56 for hematological and serum biochemical analysis. Blood samples meant for serum analysis were centrifuged at 3500 rpm for 10 minutes to get serum free of blood cells. The hematological parameters that were measured were as follows: total leukocyte count (TLC), neutrophils, lymphocytes, monocytes, red blood cell count (RBC), hemoglobin, hematocrit (HCT), MCH and platelet count.

Serum Biochemical Analysis: Serum biochemical analysis was carried out on Days 1, 14, 28, 42, and 56. The parameters measured for liver function were: aspartate transaminase (AST), alanine transaminase (ALT), alkaline phosphatase (ALP), total bilirubin, albumin, and total proteins. The activity of AST was determined through a working solution of the enzyme reagent with 20 µL of sample taken and absorbance reading done at 1, 2, and 3 minutes. ALT activity was determined through an enzymatic reaction method. ALP activity was measured using the corresponding working reagent and timed absorbance procedure. For bilirubin determination, 1000 µL distilled water and the sample were mixed with 100 µL reagent, followed by incubation for 5 min (Chandor, 2006). Albumin was determined using a biuret-based procedure; samples were mixed with biuret reagent and incubated at 25°C for 30 min before absorbance measurement (Gornall *et al*., 1949). Absorbance of the test and standard samples was recorded. All readings were performed using a chemical analyzer. Temperature control was maintained throughout all procedures.

Histopathological Examination: At the completion of the 56-day experimental period, rats were humanely euthanized by cervical dislocation following adequate anesthesia, in accordance with the approved institutional rat procedure. For histopathological examination, around 2–3 mm liver tissue samples were fixed in a solution of 10% formaldehyde with phosphate-buffered saline for 24 hours, and tissue portions were also collected for gene-expression analysis. Then, they were shifted to 70% isopropyl alcohol before soaking in 80% isopropyl alcohol for 180 minutes, and 90% and 100% for 2 hours each. After 90 minutes in acetone, the tissue was placed in xylene. In L-block tubes, dried tissue was immersed in molten paraffin wax at 58–60°C and allowed to dry. The tissue was cut with a microtome to a thickness of 5 µm and was placed on a slide containing Mayer's albumin solution (egg white in glycerol (equal volume)) containing 1% sodium salicylate for 2 hours at 60°C. Then, the tissue was deparaffinized with xylene for 20–30 minutes. Tissue sections were rehydrated by sequential immersion in decreasing concentrations of isopropyl alcohol, with each step carried out for 2–3 minutes. The tissue was soaked in water for 3 minutes, then placed in hematoxylin stain for 2 minutes, after that cleaned in tap water for 2 minutes. The mounted tissue was exposed to HCl for 1 minute, Scott's water (20 g magnesium sulfate, 3.5 g sodium carbonate, and 1 litre deionized water) for 1 minute, and eosin stain for 30 seconds. The tissue was allowed to dry by soaking it in xylene in ascending order of isopropyl alcohol for 20–30 minutes. One drop of polystyrene xylene dibutyl phthalate mounting medium was applied to the slide and allowed to dry overnight. Finally, the slides were examined under a 100x light microscope. (Mohamadnejad *et al*., 2010).

Histological Activity Index: Hepatic necro-inflammatory activity was assessed using the modified Histological Activity Index (HAI/Ishak scoring system) (Mohamadnejad *et al*., 2010). The following histopathological components were evaluated: interface hepatitis; confluent necrosis; focal/spotty lytic necrosis, apoptosis, and focal inflammatory activity; and portal inflammatory infiltration. Each component was scored according to the predefined criteria, and the component scores were summed to obtain the total HAI score, with a maximum attainable score of 18. The scoring criteria used in the study were maintained as follows:

- Interface hepatitis: 0–4
- Confluent necrosis: 0–6

- Focal/spotty lytic necrosis, apoptosis and focal inflammatory activity: 0–4
- Portal inflammatory infiltration: 0–4

The total score was calculated by summing the four component scores.

Hepatic Fibrosis Assessment: Hepatic fibrosis was evaluated using the modified Laennec scoring system, which categorizes fibrosis and cirrhosis according to septal morphology and nodular architecture. The scoring system used in the study comprised:

- Stage 0 / score 0: no fibrosis;
- Stage 1 / score 1: minimal fibrosis;
- Stage 2 / score 2: mild fibrosis;
- Stage 3 / score 3: moderate fibrosis;
- Stage 4A / score 4: early/probable cirrhosis;
- Stage 4B / score 5: moderate cirrhosis; and
- Stage 4C / score 6: advanced cirrhosis.

Stage 0 was defined as having no histological evidence of fibrosis. Minimal fibrosis was characterized by rare thin septa or absence of septa with possible mild sinusoidal fibrosis or portal-tract expansion. Higher stages were determined according to the presence and severity of fibrous septa and nodular architectural changes.

Gene Expression Analysis: Regarding gene-expression analysis, 200 mg of rat liver tissue was employed for total RNA isolation from TRIzol™ according to the procedure described previously (Rio *et al*., 2010). First, tissue was homogenized in TRIzol reagent and then kept at room temperature for 5 min. Chloroform solution was added to samples and samples were centrifuged at 12,000 rpm for 15 min at 4°C to achieve phase separation. After that, the upper aqueous phase enriched with RNA was transferred into a new RNase-free tube. Equal volumes of isopropanol were added to the aqueous phase and incubated at 25°C for 10 min, followed by centrifugation. RNA pellet was precipitated in 75% ethanol solution and spun down at 7,500 rpm. Then, RNA pellet was dried and dissolved in RNase-free water. The dissolved RNA was incubated at 56°C for 10 min to achieve full dissolution. The isolated RNA was stored at −20°C. The concentration and purity of RNA were estimated using a NanoDrop 2000 spectrophotometer.

cDNA Synthesis: The complementary DNA (cDNA) was produced from the RNA obtained from the samples by using the RevertAid First Strand cDNA Synthesis Kit as per the manufacturer's protocol. The cDNA thus produced was then used for quantitative real time PCR (qRT-PCR). The successful cDNA production was ascertained by amplification of the GAPDH reference gene and further analyzed by agarose gel electrophoresis (Kube *et al*., 2007). GAPDH was used as the housekeeping gene for the purpose of normalization due to its constitutive and stable expression in the hepatic tissues of the rats and its extensive use in liver qPCR studies. The stability of GAPDH as the normalization control gene was also confirmed by the lack of variation in the raw Ct value of the gene between the groups (one-way ANOVA, $p > 0.05$), suggesting that GAPDH expression was not affected by MTX toxicity and treatments.

Primer Design and Quantitative Real-Time PCR: Primers for ***TGF-β*** were used with the following sequences: forward primer, **GTTCCAGGGAGCCACAAAAC**; and reverse primer, **TGACATCCGGTTCGTCTACA**. Primers for ***TIMP1*** were designed using Primer3 software based on the *Rattus norvegicus* ***TIMP1*** transcript (GenBank accession **NM_053819.1**) and evaluated for primer specificity and sequence characteristics using OligoCalc. The *TIMP1* forward primer was **5′-GACCTATAGTGCTGGCTGTG-3′**, and the reverse primer was **5′-GATCGCTCTGGTAGCCCTTC-3′**, generating an expected amplicon of **134 bp** (Borah, 2011). The annealing temperature used in *TIMP1* amplification was 58°C. For each sample, separate qRT-PCR reactions were conducted for *TIMP1*, *TGF-β*, and GAPDH. Each reaction included cDNA, gene-specific primers for forward and reverse directions, and PowerUp™ SYBR™ Green Master Mix, according to the instructions provided by the company. PCR products were detected by SYBR Green fluorescence, and melting curve analysis was conducted after amplification for the specificity of the PCR products

qPCR Amplification Efficiency: The efficiency of the qRT-PCR reaction was assessed using the standard curve that was constructed on the basis of diluted pooled cDNA. Experimental standard curve revealed a linear correlation between Ct values and the logarithm of template concentration, with $R^2 = 0.997$ and slope = −3.587. Amplification efficiency was calculated from the standard-curve slope using the following equation:

E = 10^(−1/slope) − 1

When expressed as a percentage:

Amplification efficiency (%) = [10^(−1/slope) − 1] × 100

Using a slope of **−3.587**, the calculated amplification efficiency is approximately **90%**.

Relative Gene Expression Analysis: Relative gene expression of ***TIMP1*** and ***TGF-β*** was determined using the comparative **2^−ΔΔCt method** described by Livak and Schmittgen. GAPDH was used as the endogenous reference gene, and the normal-control group served as the calibrator (Livak and Schmittgen, 2001). For each biological sample, the difference between the Ct value of the target gene and that of GAPDH was calculated as:

$$\Delta Ct = Ct\ (target\ gene) - Ct\ (GAPDH)$$

The ΔCt of each experimental sample was then compared with the mean ΔCt of the calibrator group:

$$\Delta\Delta Ct = \Delta Ct\ (experimental\ sample) - \Delta Ct\ (calibrator/control\ group)$$

Relative gene expression was calculated as: **Relative expression (fold change) = 2^−ΔΔCt**

The normal-control group was assigned a relative expression value of **1.0** and used as the calibrator. Individual rats were considered the biological experimental units. Where technical PCR replicates were performed, the Ct values from the technical replicates were averaged for each biological sample before calculation of ΔCt and subsequent relative expression. Statistical testing was performed on ΔCt values, whereas 2^-ΔΔCt values were presented for biological interpretation.

Statistical Analysis: All statistical analyses were performed using SPSS software, version 26.0. Quantitative data were summarized as mean ± standard error of the mean (SEM). Prior to parametric analysis, the assumptions of normality and homogeneity of variance were assessed. Because hematological and biochemical parameters were measured repeatedly in the same experimental rats at Days 1, 14, 28, 42, and 56, a two-way mixed-design repeated-measures analysis of variance (ANOVA) was performed. Treatment group was specified as the between-subject factor, while time was specified as the within-subject (repeated-measures) factor. The treatment × time interaction was evaluated to determine whether changes over time differed among treatment groups. The analysis therefore assessed the main effects of treatment group and time, as well as their interaction. Individual rats were treated as the experimental subjects for the repeated measurements. Day 1 was considered the baseline/pre-treatment assessment, whereas Days 14, 28, 42, and 56 represented subsequent treatment assessments. Where statistically significant effects were identified, appropriate post-hoc pairwise comparisons with multiple-comparison adjustment were performed. Effect size was estimated using partial eta-squared (ηp^2) where applicable. A p-value ≤ 0.05 was considered statistically significant. The complete repeated-measures ANOVA results, including the main effects of treatment and time and the treatment × time interaction, are presented in the supplementary statistical analysis/appendices (Mishra *et al*., 2019). Histopathological HAI and Laennec fibrosis scores were terminal outcomes and were therefore analyzed separately according to the statistical method specified for the ordinal/discrete histopathological data. For qRT-PCR analysis, individual rats were considered the biological replicates, and relative-expression values were analyzed according to the experimental group structure.

RESULTS

The results confirmed the physicochemical characterization of metformin-loaded chitosan nanoparticles, followed by the evaluation of their hepatoprotective potential in a methotrexate-induced liver injury model. Assessment of hematological parameters, liver function biomarkers, histopathological features, fibrosis scores, and the expression of fibrosis-associated genes demonstrated that nanoparticle-based metformin treatment effectively attenuated methotrexate-induced hepatic injury.

Characterization of Metformin-Loaded Chitosan Nanoparticles (Met-CSNPs): The prepared Met-CSNPs were successfully characterized using Fourier-transform infrared spectroscopy (FTIR), scanning electron microscopy (SEM), dynamic light scattering (DLS), zeta-potential analysis, drug-entrapment assessment, and an *in vitro* drug-release study.

FTIR Spectral Analysis: The FTIR spectrum demonstrated characteristic absorption bands associated with the chitosan nanoparticle formulation (Figure 2a). A prominent band at approximately 3447 cm^{-1} was attributed mainly to the stretching vibrations of the $–NH_2$ and –OH functional groups, and a further characteristic band at approximately 1639 cm^{-1} corresponded to the amide-associated region. The observed chitosan-associated peaks, together with the absence of unexpected additional prominent peaks, supported successful formation of the nanoparticle formulation without evidence of major extraneous spectral components.

Scanning Electron Microscopy: SEM examination demonstrated that the nanoparticles were predominantly spherical and relatively uniform in morphology (Figure 2b). The average particle size observed by SEM was approximately 200 nm. Some aggregation was observed after prolonged maintenance of the particles in suspension, indicating a tendency for particle aggregation during extended storage.

Particle Size, Polydispersity, and Zeta Potential: Dynamic Light Scattering analysis demonstrated an average nanoparticle size of approximately 213 nm with a low polydispersity index of approximately 0.30, indicating a relatively

narrow particle-size distribution (Figure 2c). The mean zeta potential was +28.1 mV (Figure 2d). The principal intensity peak was approximately 195.65 nm, with a smaller secondary peak at approximately 11.9 nm, and the mean intensity was approximately 81.6 kcounts/s. Overall, the physicochemical measurements confirmed the formation of nanosized particles carrying a positive surface charge.

Drug Entrapment Efficiency: The metformin entrapment efficiency was 97.34% (Figure 2e). Of the 10 mg metformin initially used in the formulation, 0.266 mg of free, unentrapped drug was detected in the supernatant following centrifugation; the calculated amount incorporated into the nanoparticles was therefore 9.734 mg, corresponding to an entrapment efficiency of 97.34%. These findings demonstrated a high degree of metformin incorporation into the chitosan nanoparticle formulation. Nanoparticle doses were expressed as mg/kg/day of the total Met-CSNP formulation.

***In Vitro* Drug-Release Profile:** The *in vitro* release profile demonstrated a progressive, time-dependent release of metformin from the chitosan nanoparticles over 24 h (Figure 2f). Approximately 15% of the drug was released during the first hour, increasing to 28% at 2 h, 45% at 4 h, 62% at 6 h, and 75% at 8 h. Cumulative release reached approximately 90% at 12 h and 100% at 24 h, consistent with a sustained release pattern.

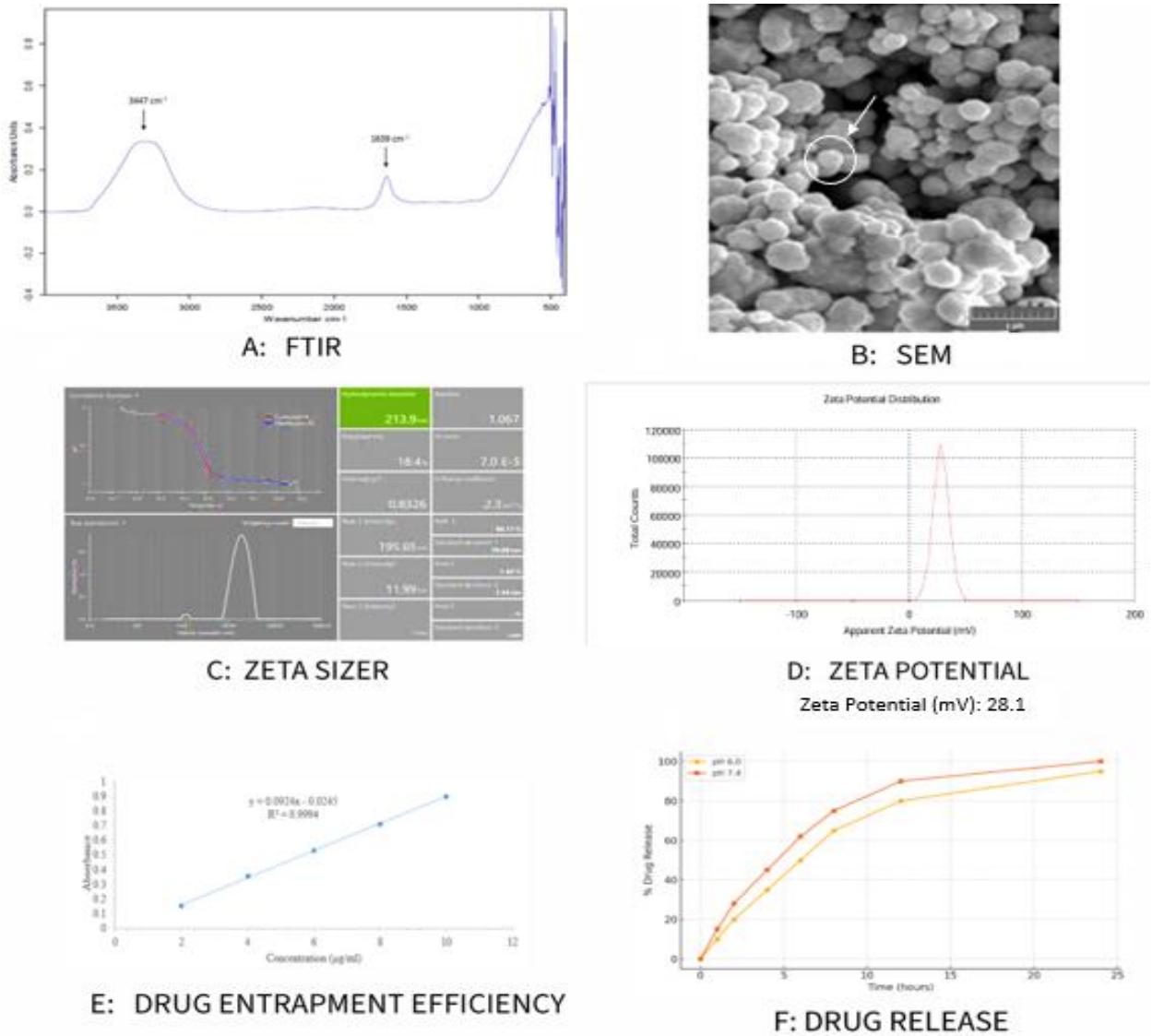

Figure 2. Characterization of Met-CSNPs: (a) FTIR spectrum, (b) SEM morphology, (c) particle-size distribution, (d) zeta-potential distribution, (e) drug-entrapment assessment, and (f) *in vitro* drug-release profile.

Baseline Comparability: Before treatment (Day 1), one-way ANOVA revealed no statistically significant differences among the eight groups for any hematological or serum-biochemical parameter (all $p \geq 0.208$), with correspondingly small effect sizes (partial eta-squared, $\eta p^2 \leq 0.204$). Representative baseline comparisons included RBC ($F(7,40) = 0.98$, $p = 0.457$), hemoglobin ($F(7,40) = 0.11$, $p = 0.998$), platelets ($F(7,40) = 1.29$, $p = 0.280$), AST ($F(7,40) = 0.33$, $p = 0.934$), ALT ($F(7,40) = 0.66$, $p = 0.708$), and bilirubin ($F(7,40) = 0.27$, $p = 0.963$). No statistically significant baseline differences were detected among the experimental groups. Model assumptions were examined before the repeated-measures analyses. Mauchly's test indicated that the sphericity assumption was violated for the within-subject (time) factor for all fifteen parameters ($p \leq 0.001$); accordingly, the Greenhouse–Geisser correction was applied to both the time main effect and the treatment × time interaction for every parameter, and effect sizes are reported throughout as partial eta-squared (ηp^2). Levene's test supported homogeneity of between-group variance for all parameters except ALT, for which variances were heterogeneous (median-centred Levene $p = 0.005$ at Day 56; $p \leq 0.001$ across the full longitudinal series).

Hematological Findings: Significant treatment effects were observed for all nine hematological parameters (all $p \leq 0.001$), while significant time effects and treatment × time interactions were observed for all parameters, with p-values ranging from ≤0.001 to 0.034. The treatment effect was large for every parameter, with partial ηp^2 values ranging from 0.855 (monocytes) to 0.971 (lymphocytes), indicating that treatment allocation accounted for a substantial proportion of the observed variance. The significant interaction terms confirm that the trajectories of the hematological parameters over Days 1–56 differed among the treatment groups.

Table 1. Two-way repeated-measures ANOVA for hematological parameters.

Parameter	Effect	F (df1, df2)	p	Partial ηp^2	Correction
RBC	Treatment	F (7, 40) = 92.03	≤0.001	0.942	—
	Time	F (1.4, 55.0) = 139.87	≤0.001	0.781	GG (ε = 0.344)
	Treatment × Time	F (28, 160) = 20.40	≤0.001	0.781	—
Hemoglobin	Treatment	F (7, 40) = 95.22	≤0.001	0.943	—
	Time	F (1.4, 54.7) = 132.02	≤0.001	0.772	GG (ε = 0.342)
	Treatment × Time	F (28, 160) = 15.12	≤0.001	0.726	—
HCT	Treatment	F (7, 40) = 54.49	≤0.001	0.905	—
	Time	F (1.4, 56.8) = 161.88	≤0.001	0.800	GG (ε = 0.355)
	Treatment × Time	F (28, 160) = 18.30	≤0.001	0.762	—
MCH	Treatment	F (7, 40) = 45.46	≤0.001	0.888	—
	Time	F (1.8, 72.1) = 72.26	≤0.001	0.643	GG (ε = 0.451)
	Treatment × Time	F (28, 160) = 7.49	≤0.001	0.567	—
TLC	Treatment	F (7, 40) = 78.51	≤0.001	0.932	—
	Time	F (1.3, 53.2) = 115.54	≤0.001	0.738	GG (ε = 0.333)
	Treatment × Time	F (28, 160) = 15.53	≤0.001	0.731	—
Neutrophils (%)	Treatment	F (7, 40) = 113.12	≤0.001	0.952	—
	Time	F (1.3, 52.3) = 53.31	≤0.001	0.570	GG (ε = 0.327)
	Treatment × Time	F (28, 160) = 23.39	≤0.001	0.804	—
Lymphocytes (%)	Treatment	F (7, 40) = 188.19	≤0.001	0.971	—
	Time	F (4, 160) = 129.00	0.001	0.763	
	Treatment × Time	F (28, 160) = 12.25	<0.001	0.682	
Monocytes (%)	Treatment	F (7, 40) = 33.83	≤0.001	0.855	—
	Time	F (4, 160) = 19.11	0.022	0.323	
	Treatment × Time	F (28, 160) = 5.40	0.002	0.486	
Platelets	Treatment	F (7, 40) = 69.22	≤0.001	0.924	—
	Time	F (4, 160) = 235.20	≤0.001	0.855	
	Treatment × Time	F (28, 160) = 2.97	0.034	0.342	

GG, Greenhouse–Geisser correction (ε = Greenhouse–Geisser epsilon); degrees of freedom for corrected terms are reported as adjusted values. A p-value ≤ 0.05 was considered significant.

At the terminal assessment (Day 56), the MTX toxic control (Group B) showed the most severe hematological disturbance. Erythroid indices were markedly reduced in Group B relative to the normal control (Group A): RBC fell to $3.67 \pm 0.46 \times 10^{12}$/L (vs 8.10 ± 0.45 in Group A), hemoglobin to 9.8 ± 0.7 g/dL (vs 15.4 ± 0.6), and HCT to 32.0 ± 2.2% (vs 47.5 ± 1.8), whereas MCH was elevated to 23.58 ± 0.97 pg (vs 18.6 ± 0.7). Treatment with Met-CSNPs produced a clear dose-dependent restoration of these indices: RBC rose progressively across Groups F (6.05 ± 0.50), G (6.60 ± 0.48), and H (7.70 ± 0.45), and the high-dose group (H) approached the normal-control and blank-nanoparticle (C, 7.85 ± 0.45) values. Hemoglobin and HCT followed the same pattern, with Group H (14.8 ± 0.6 g/dL; 46.8 ± 1.8%) and Group G (14.3 ± 0.6 g/dL; 43.0 ± 1.8%) showing the strongest recovery, while free metformin (Group E) was the least effective among the active treatments (11.5 ± 0.7 g/dL; 36.5 ± 2.0%). MCH normalized in a dose-dependent manner, with Group H (18.9 ± 0.7 pg) closest to the normal control. All group-versus-B comparisons for RBC, hemoglobin, HCT, and MCH were statistically significant (Bonferroni-adjusted $p \leq 0.036$). Leukocyte and platelet parameters showed a comparable pattern. Total leukocyte count (TLC) was suppressed in Group B ($5.2 \pm 0.7 \times 10^9$/L vs 11.8 ± 0.9 in Group A) and was strongly restored by silymarin (Group D, 10.6 ± 0.9) and by the high-dose nanoparticle formulation (Group H, 10.2 ± 0.9), with partial recovery at the intermediate dose (Group G, 8.8 ± 0.8). In contrast, free metformin (Group E, 6.0 ± 0.7) and the low-dose nanoparticles (Group F, 6.4 ± 0.7) remained close to the toxic-control value, and neither differed significantly from Group B after adjustment (E vs B, $p = 0.389$; F vs B, $p = 0.077$). Neutrophil percentage was increased in Group B (32.0 ± 2.3% vs 20.0 ± 1.8%) and was highest in the silymarin group (Group D, 36.0 ± 2.4%; D vs B, $p = 0.009$), whereas the nanoparticle groups moved toward the normal range, with Group G (21.0 ± 1.9%) closest to control. Lymphocyte percentage was lowest in Group B (55.0 ± 4.0% vs 72.0 ± 3.0%) and was fully restored in the intermediate- and high-dose nanoparticle groups (G and H, 71.0 ± 3.0% each) and highest in the blank-nanoparticle group (C, 78.0 ± 3.0%); the silymarin group did not differ significantly from Group B (D vs B, $p = 0.467$). Monocyte percentage was elevated in Group B (6.5 ± 0.9% vs 3.0 ± 0.5%) and decreased dose-dependently, being lowest in Groups C (2.8 ± 0.5%) and H (3.2 ± 0.5%). Platelet count was markedly reduced in Group B ($430 \pm 45 \times 10^9$/L vs 980 ± 60 in Group A) and recovered in a clearly dose-dependent fashion across the nanoparticle groups: F (470 ± 48) < G (650 ± 60) < H (820 ± 65). The blank-nanoparticle group showed the highest count (C, 1010 ± 60). All group-versus-B platelet comparisons were significant except the low-dose nanoparticle group (F vs B, $p = 0.738$). Overall, the hematological data indicate pronounced MTX-induced myelosuppression that was attenuated in a dose-dependent manner by the Met-CSNPs, with the 75 mg/kg/day formulation (Group H) producing the most complete recovery among the nanoparticle treatments.

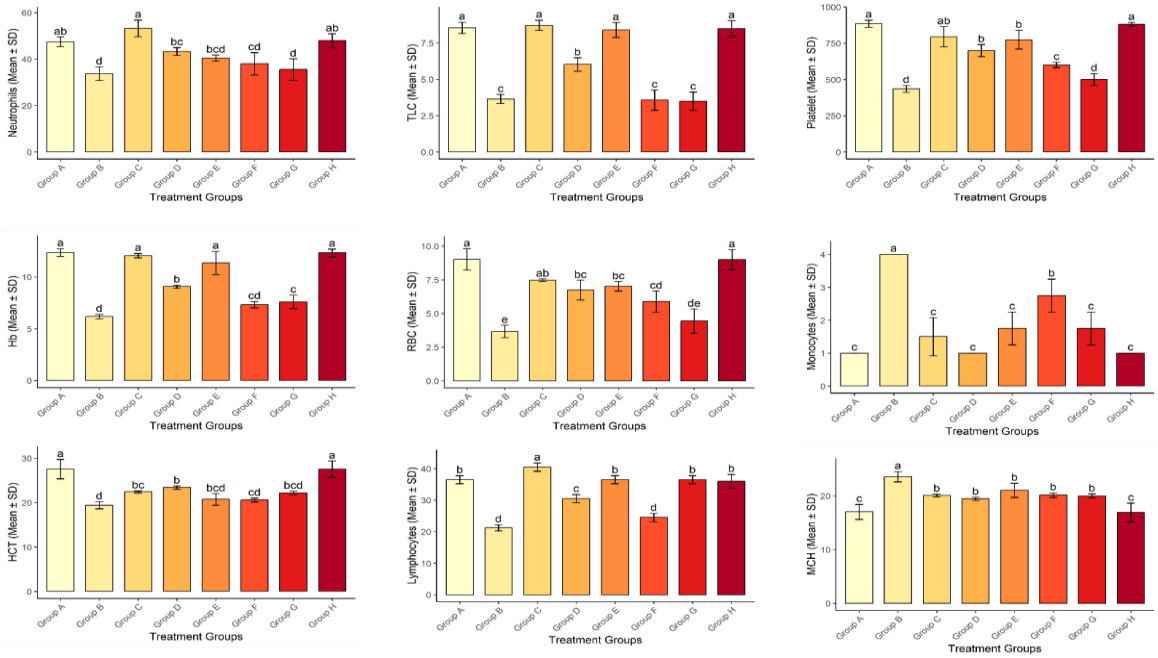

Figure 3. Comparison of hematological parameters among the experimental groups at the terminal assessment, including neutrophils, TLC, platelets, hemoglobin, RBC, monocytes, HCT, lymphocytes, and MCH.

Serum Biochemical Findings: Two-way repeated-measures ANOVA demonstrated significant main effects of treatment and time and a significant treatment × time interaction for all six liver-function parameters (Table 2). The treatment effect was very large in every case, with partial ηp^2 values ranging from 0.946 (ALT) to 0.991 (total protein), confirming that the between-group differences accounted for the majority of the variance in the biochemical outcomes.

Table 2. Two-way repeated-measures ANOVA for serum biochemical parameters.

Parameter	Effect	F (df1, df2)	p	Partial ηp^2
Bilirubin	Treatment	F (7, 40) = 377.77	≤0.001	0.985
	Time	F (4, 160) = 25.57	≤0.001	0.390
	Treatment × Time	F (28, 160) = 22.33	≤0.001	0.796
AST	Treatment	F (7, 40) = 446.52	≤0.001	0.987
	Time	F (4, 160) = 54.76	≤0.001	0.578
	Treatment × Time	F (28, 160) = 83.92	≤0.001	0.936
ALT	Treatment	F (7, 40) = 99.54	≤0.001	0.946
	Time	F (4, 160) = 93.10	≤0.001	0.699
	Treatment × Time	F (28, 160) = 53.54	≤0.001	0.904
ALP	Treatment	F (7, 40) = 232.16	≤0.001	0.976
	Time	F (4, 160) = 53.29	≤0.001	0.571
	Treatment × Time	F (28, 160) = 42.59	≤0.001	0.882
Total protein	Treatment	F (7, 40) = 651.89	≤0.001	0.991
	Time	F (4, 160) = 9.50	0.004	0.192
	Treatment × Time	F (28, 160) = 6.64	≤0.001	0.537
Albumin	Treatment	F (7, 40) = 127.17	≤0.001	0.957
	Time	F (4, 160) = 18.48	≤0.001	0.316
	Treatment × Time	F (28, 160) = 13.22	≤0.001	0.698

The F statistic and p-value for each term test the main effect of treatment, the main effect of sampling time, and the treatment × time interaction, respectively. A p-value ≤ 0.05 was considered significant.

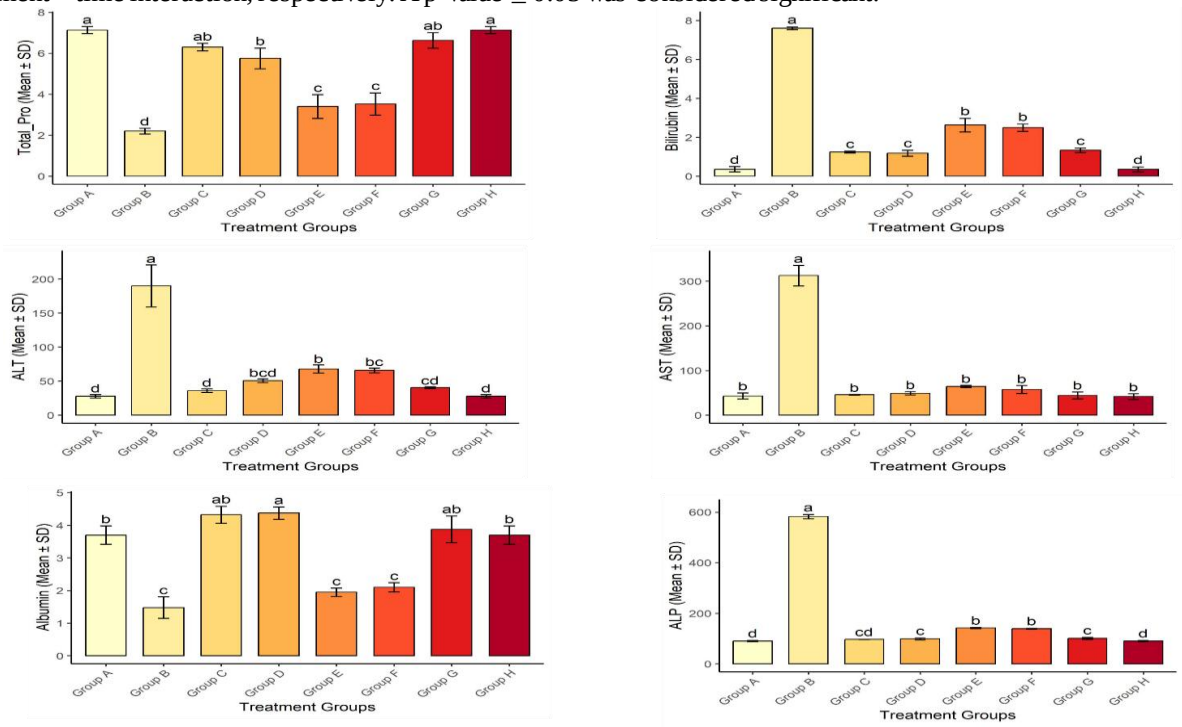

Figure 4. Comparison of serum biochemical parameters among the experimental groups at the terminal assessment, including AST, ALT, ALP, bilirubin, total protein, and albumin.

At Day 56, MTX administration (Group B) produced marked hepatocellular injury and cholestasis. Serum AST rose to 312.5 ± 22.88 U/L (vs 82.0 ± 6.0 in Group A), ALT to 190.0 ± 30.82 U/L (vs 44.0 ± 4.0), ALP to 582.59 ± 7.99 U/L (vs 155.0 ± 10.0), and total bilirubin to 7.61 ± 0.07 mg/dL (vs 0.42 ± 0.04). All active treatments significantly lowered these markers relative to Group B (adjusted $p \leq 0.001$ throughout), and the response was consistently dose-dependent for the nanoparticle formulations. AST decreased across Groups F (145.0 ± 11.0), G (118.0 ± 9.0), and H (100.0 ± 8.0), with the high-dose group closest to normal; ALT was lowest in Group H (40.5 ± 1.29, approached the value observed in the normal-control group), followed by G (52.0 ± 5.0) and F (70.0 ± 7.0); and ALP declined similarly, reaching 190.0 ± 12.0 U/L in Group H. Bilirubin normalized dose-dependently, from 1.95 ± 0.15 mg/dL (F) to 1.40 ± 0.12 (G) to 0.95 ± 0.08 (H). Across these markers, free metformin (Group E) was the least effective of the active treatments (AST 178.0 ± 14.0; ALT 95.0 ± 9.0; ALP 360.0 ± 25.0; bilirubin 2.85 ± 0.20). The liver-function markers showed the reciprocal pattern. Total protein was reduced in Group B (2.20 ± 0.14 g/dL vs 7.05 ± 0.25 in Group A) and albumin fell to 1.35 ± 0.12 g/dL (vs 4.05 ± 0.18). Both recovered dose-dependently with nanoparticle treatment, with Group H showing the highest values among the nanoparticle groups (total protein 6.6 ± 0.25 g/dL; albumin 3.8 ± 0.18 g/dL) and free metformin again the least effective (total protein 4.1 ± 0.35; albumin 2.4 ± 0.25); all group-versus-B comparisons were significant (adjusted $p \leq 0.001$). The blank-nanoparticle group (C) remained comparable to the normal control for every biochemical parameter, indicating that the nanocarrier itself was not hepatotoxic. Taken together, the biochemical findings demonstrate pronounced MTX-associated hepatic dysfunction that was attenuated in a dose-dependent manner by Met-CSNPs, with the 75 mg/kg/day regimen (Group H) providing the most favorable overall profile.

Histopathological Findings: Necro-inflammatory activity was scored using the modified Ishak Histological Activity Index (HAI), and fibrosis was staged using the modified Laennec system. Because these ordinal scores were terminal outcomes, groups were compared using the Kruskal–Wallis test with Dunn's post-hoc comparisons. Both endpoints differed significantly among the eight groups (HAI: $H = 44.5$, $df = 7$, $p \leq 0.001$; Laennec fibrosis: $H = 42.65$, $df = 7$, $p \leq 0.001$; Table 3).

Table 3. Hepatic necro-inflammatory (modified Ishak HAI) and fibrosis (modified Laennec) scores by group (n = 6 per group).

Group	Treatment	Modified Ishak HAI, median (IQR)	Laennec fibrosis, median (IQR)
A	Normal control	0 (0.0–0.0)	0 (0.0–0.0)
B	MTX (toxic control)	6 (5.2–6.0)	4 (4.0–4.8)
C	Blank chitosan nanoparticles	0 (0.0–0.0)	0 (0.0–0.0)
D	MTX + silymarin	3 (3.0–3.8)	3 (2.2–3.0)
E	MTX + free metformin	3 (3.0–3.8)	3 (2.2–3.0)
F	MTX + Met-CSNP (25 mg/kg/day)	1 (1.0–1.8)	2 (2.0–2.8)
G	MTX + Met-CSNP (50 mg/kg/day)	1 (1.0–1.8)	2 (2.0–2.8)
H	MTX + Met-CSNP (75 mg/kg/day)	0 (0.0–0.8)	0 (0.0–0.0)

IQR, interquartile range. Overall differences were tested by the Kruskal–Wallis test (HAI: $H = 44.5$, $df = 7$, $p \leq 0.001$; Laennec: $H = 42.65$, $df = 7$, $p \leq 0.001$).

Groups A and C showed fully preserved hepatic architecture, with all four HAI components (interface hepatitis, confluent necrosis, focal necrosis, and portal inflammation) scored 0 in 6/6 rats and Laennec stage 0 in every rat. In contrast, the MTX toxic control (Group B) exhibited severe injury: confluent (zone 3) necrosis was scored 3 in 6/6 rats and portal inflammation 2 in 6/6 rats, giving a total HAI of 6 in 4/6 rats and 5 in 2/6 rats, with advanced fibrosis (Laennec stage 4 in 4/6 rats and stage 5 in 2/6 rats). Silymarin (Group D) and free metformin (Group E) produced partial attenuation, with confluent necrosis of 1 in 4/6 and 2 in 2/6 rats, portal inflammation of 1 in 4/6 and 2 in 2/6 rats, a total HAI of 3 in 4/6 and 4 in 2/6 rats, and fibrosis of stage 3 in 4/6 and stage 2 in 2/6 rats. The metformin-loaded chitosan nanoparticle groups showed progressively greater tissue preservation. Groups F and G reduced confluent necrosis to a score of 1 in 6/6 rats and portal inflammation to 0 in 4/6 and 1 in 2/6 rats, yielding a total HAI of 1 in 4/6 and 2 in 2/6 rats and fibrosis of stage 2 in 4/6 and stage 3 in 2/6 rats. The high-dose group (Group H) demonstrated the most favorable pattern: confluent necrosis was absent (score 0 in 6/6), portal inflammation was absent to minimal (0 in 4/6 and 1 in 2/6), the total HAI was 0 in 4/6 and 1 in 2/6 rats, and no fibrosis was detected (Laennec stage 0 in 6/6). Dunn's post-hoc analysis confirmed that HAI was significantly lower than the MTX toxic control in Groups A, C, F, G, and H (adjusted $p \leq 0.024$), whereas silymarin and free metformin did not reach significance versus Group B (D vs B and E vs

B, adjusted p = 0.506). For fibrosis, only Groups A, C, and H were significantly lower than Group B (adjusted p ≤ 0.001); the reductions seen with silymarin, free metformin, and the low- and intermediate-dose nanoparticles did not reach significance after multiplicity adjustment (adjusted p ≥ 0.112). Thus, among all treatments the 75 mg/kg/day nanoparticle formulation was the only regimen to significantly reduce hepatic fibrosis relative to MTX.

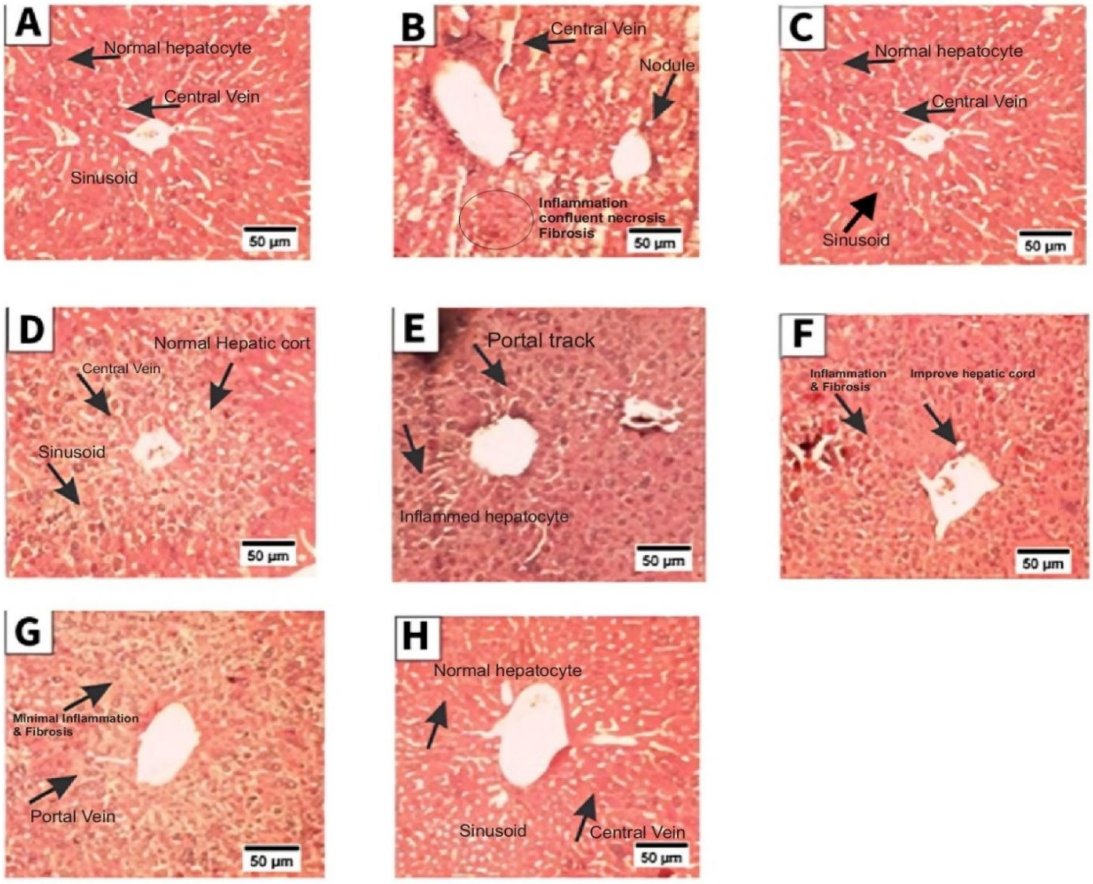

Figure 5. Representative H & E-stained liver sections from the experimental groups after the treatment period (100× magnification), evaluated using the modified Ishak HAI and Laennec fibrosis staging systems.

Gene-Expression Analysis

RNA Quality and cDNA Confirmation: Total RNA extracted from liver tissue showed acceptable purity, with most samples yielding A260/280 ratios close to 1.9. Successful cDNA synthesis was confirmed by amplification of the GAPDH reference transcript, which produced a distinct band of approximately 550 bp on agarose gel electrophoresis (Figure 6). The raw GAPDH Ct values were uniform across all experimental groups, supporting its suitability as a stable normalization reference. Relative expression of *TIMP1* and *TGF-β* was quantified by the comparative $2^{-\Delta\Delta Ct}$ method with GAPDH as the reference gene and the normal control (Group A) as the calibrator (assigned a value of 1.0). One-way ANOVA on the ΔCt values confirmed significant between-group differences for both genes (*TIMP1*: F (7,40) = 93.89, p ≤ 0.001, $\eta p^2 = 0.943$; *TGF-β*: F (7,40) = 126.56, p ≤ 0.001, $\eta p^2 = 0.957$). Group-wise fold-change values and Dunnett comparisons against the normal control are summarized in Table 4.

***TIMP1* Expression:** MTX administration markedly upregulated hepatic *TIMP1* expression, which reached 6.77-fold in the toxic control (Group B) relative to the normal control. Every treatment reduced *TIMP1* expression below the Group B level. Silymarin (Group D) produced the lowest expression overall (0.62-fold), followed by the high and intermediate-dose nanoparticle groups (H, 1.74-fold; G, 1.87-fold) and the blank-nanoparticle group (C, 1.93-fold). The low-dose nanoparticles (F, 3.89-fold) and free metformin (E, 3.05-fold) were less effective. Among the metformin-loaded nanoparticle formulations, 75 mg/kg/day dose (Group H) achieved the greatest suppression of *TIMP1*. All groups differed significantly from the normal control (Dunnett-adjusted p ≤ 0.001), consistent with residual expression above the calibrator baseline in the treated groups. Notably, *TIMP1* expression across the three nanoparticle doses was

monotonic with dose (25 mg/kg, 3.89-fold; 50 mg/kg, 1.87-fold; 75 mg/kg, 1.74-fold); the response is therefore described as dose-dependent.

Table 4. Relative hepatic expression of *TIMP1* and *TGF-β* (2−ΔΔCt method; n = 6 per group).

Gene	Group	Treatment	2−ΔΔCt (fold)	Adj. p vs A
TIMP1	A	Normal control	1.00	calibrator
TIMP1	B	MTX (toxic control)	6.77	≤0.001
TIMP1	C	Blank chitosan nanoparticles	1.93	≤0.001
TIMP1	D	MTX + silymarin	0.62	≤0.001
TIMP1	E	MTX + free metformin	3.05	≤0.001
TIMP1	F	MTX + Met-CSNP (25 mg/kg/day)	3.89	≤0.001
TIMP1	G	MTX + Met-CSNP (50 mg/kg/day)	1.87	≤0.001
TIMP1	H	MTX + Met-CSNP (75 mg/kg/day)	1.74	≤0.001
TGF-β	A	Normal control	1.00	calibrator
TGF-β	B	MTX (toxic control)	4.66	≤0.001
TGF-β	C	Blank chitosan nanoparticles	0.81	0.330
TGF-β	D	MTX + silymarin	0.69	0.017
TGF-β	E	MTX + free metformin	5.90	≤0.001
TGF-β	F	MTX + Met-CSNP (25 mg/kg/day)	3.05	≤0.001
TGF-β	G	MTX + Met-CSNP (50 mg/kg/day)	1.57	0.002
TGF-β	H	MTX + Met-CSNP (75 mg/kg/day)	0.51	≤0.001

Fold change is expressed relative to the normal control (Group A). p-values are Dunnett-adjusted comparisons against Group A. A p-value ≤ 0.05 was considered significant. p-values were calculated from statistical comparisons of ΔCt values; fold changes are presented as 2^-ΔΔCt for descriptive interpretation.

***TGF-β* Expression:** Hepatic *TGF-β* expression was also elevated by MTX, reaching 4.66-fold in Group B. The response to treatment was formulation-dependent and, notably, discordant with the *TIMP1* pattern. The high-dose nanoparticle group (H) produced the greatest suppression of any group, reducing expression to 0.51-fold of the normal control, while silymarin (D, 0.69-fold) and the blank nanoparticles (C, 0.81-fold) were similarly low; the blank-nanoparticle group did not differ significantly from the normal control (adjusted p = 0.330). The low- and intermediate-dose nanoparticles gave 3.05-fold (F) and 1.57-fold (G) expression, respectively. In contrast, free metformin (Group E) increased *TGF-β* expression to 5.90-fold—higher than the MTX toxic control itself. As with *TIMP1*, *TGF-β* expression across the nanoparticle doses was monotonic (25 mg/kg, 3.05-fold; 50 mg/kg, 1.57-fold; 75 mg/kg, 0.51-fold), so the effect is characterized as graded dose–response. Thus, the 75 mg/kg/day nanoparticle formulation (Group H) produced the strongest reduction in this pro-fibrotic mediator, whereas non-encapsulated metformin failed to attenuate, and in fact amplified, the *TGF-β* response.

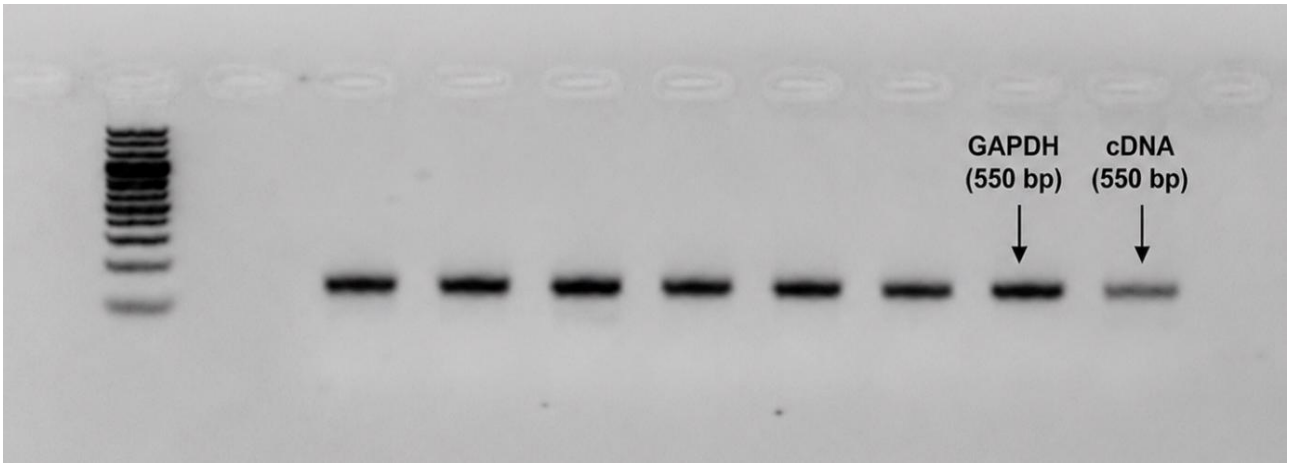

Figure 6. Confirmation of cDNA synthesis by agarose gel electrophoresis (≈550-bp GAPDH product).

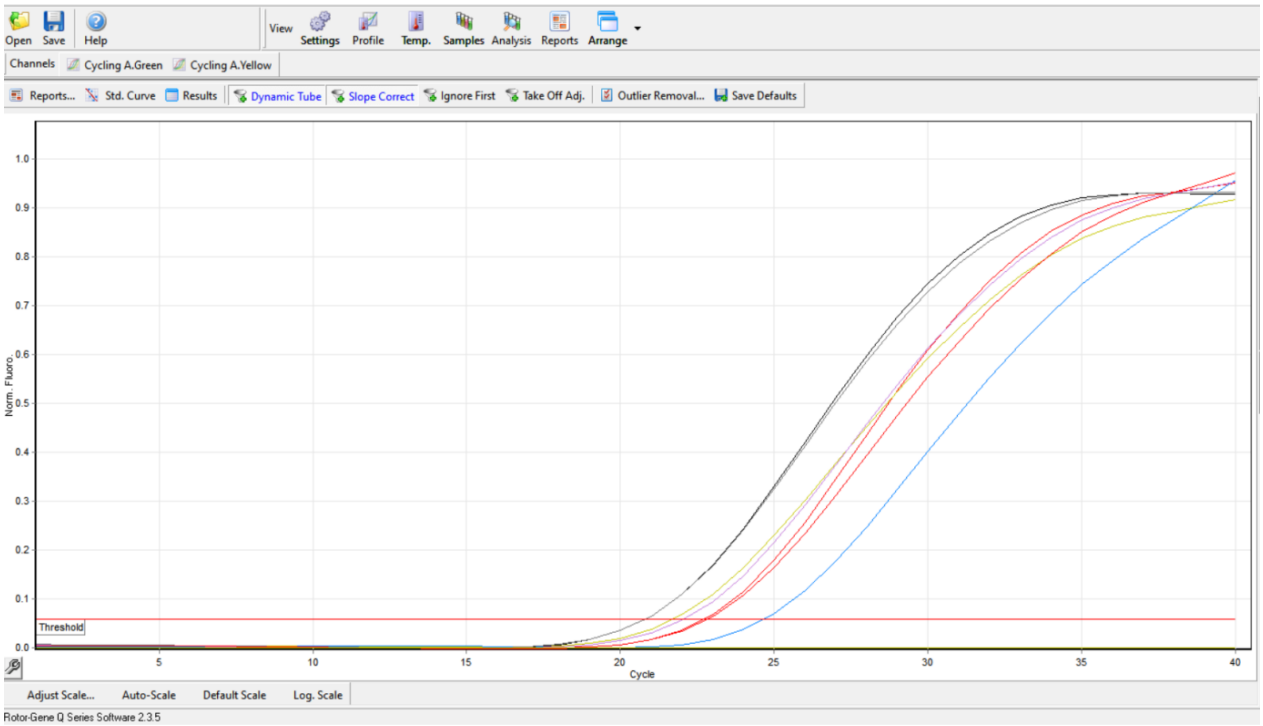

Figure 7. Representative sigmoidal amplification curves for *TIMP1* expression in liver tissue by quantitative real-time PCR.

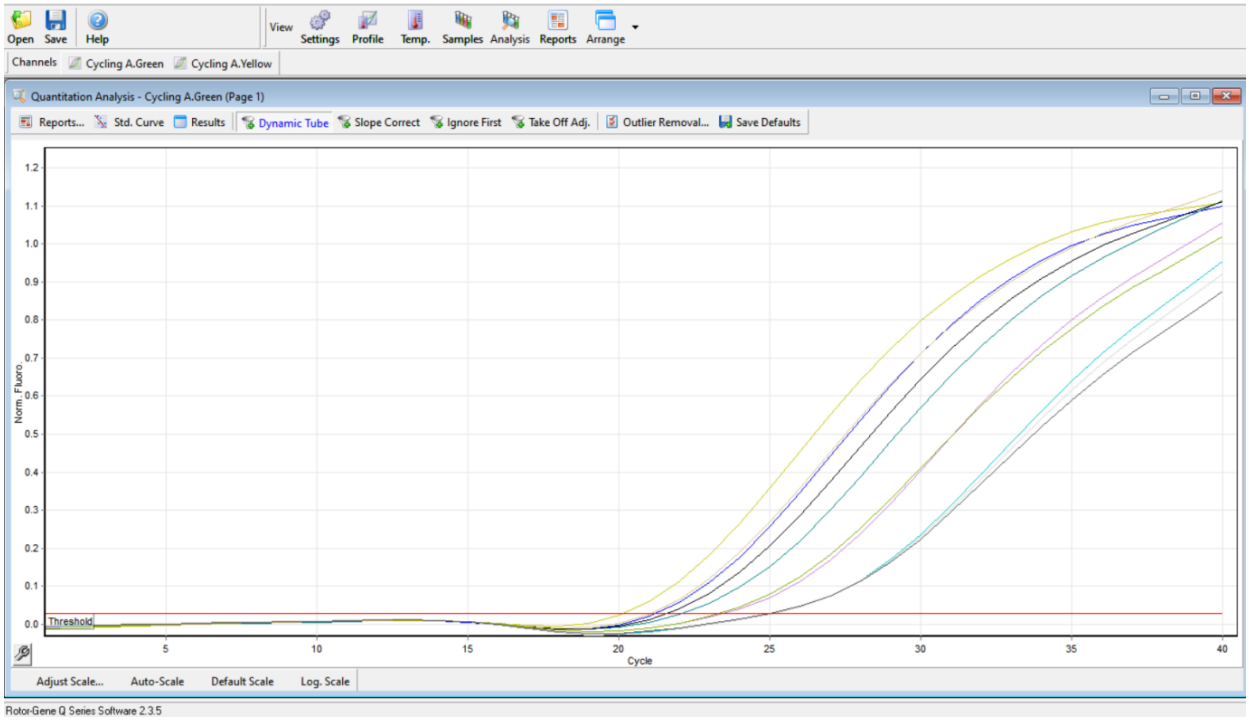

Figure 8. Representative sigmoidal amplification curves for *TGF-β* expression in liver tissue by quantitative real-time PCR.

Overall Pattern of Hepatoprotective Response: Integrating the hematological, biochemical, histopathological, and molecular data, MTX produced consistent and severe hepatic injury—myelosuppression, elevated transaminases, ALP and bilirubin with reduced total protein and albumin, extensive necro-inflammation and advanced fibrosis, and

upregulation of the pro-fibrotic mediators *TIMP1* and *TGF-β*. The blank chitosan nanoparticles (Group C) were comparable to the normal control for the biochemical, hematological, and histopathological endpoints, indicating that the carrier itself was not hepatotoxic; however, Group C was not equivalent to the normal control at every endpoint, showing a modest but statistically significant elevation of *TIMP1* (1.93-fold; Dunnett-adjusted $p \leq 0.001$), so the carrier cannot be described as biologically inert across all measures. Met-CSNPs conferred dose-dependent hepatoprotection on the biochemical and histopathological endpoints, and the 75 mg/kg/day formulation (Group H) was the strongest overall performer: it produced the most favorable biochemical profile, the lowest necro-inflammatory scores, complete absence of fibrosis (the only regimen to reduce fibrosis significantly versus MTX), and the greatest suppression of *TGF-β* (0.51-fold). Among the Met-CSNP formulations, the 75 mg/kg/day dose (Group H) achieved the greatest suppression of *TIMP1* expression. Free metformin (Group E) was consistently the least effective active treatment and paradoxically increased *TGF-β* above the toxic-control level. These findings suggest that nanoparticle-mediated delivery may enhance the hepatoprotective effects of metformin. Collectively, the molecular results reinforce the biochemical and histopathological findings and support a hepatoprotective, anti-fibro genic effect of Met-CSNPs against MTX-induced liver injury.

DISCUSSION

Methotrexate (MTX) is one of the most widely used antifolate drugs for cancer and for autoimmune conditions such as rheumatoid arthritis and psoriasis. Its long-term use is held back by liver injury, which develops through a linked set of events that includes excess reactive oxygen species, mitochondrial damage, release of inflammatory cytokines, hepatocyte apoptosis, and a gradual build-up of extracellular matrix that ends in fibrosis and, in severe cases, liver failure (Howard *et al*., 2016). A delivery system that shields the liver from this toxicity while keeping the drug effective would therefore be valuable. In the present study, metformin was loaded into chitosan nanoparticles (Met-CSNPs) and tested for protection against MTX-induced liver damage in rats. The formulation lowered MTX toxicity in a dose-related way. It improved blood counts, brought liver function markers back toward normal, preserved liver structure, reduced fibrosis, and lowered the expression of the profibrotic genes *TGF-β* and *TIMP1*. The 75 mg/kg/day dose (Group H) gave the strongest response across almost every measure, while free metformin (Group E) was the weakest of the active treatments.

FTIR analysis showed that metformin was held inside the chitosan particles without altering the chemical make-up of the polymer. The spectrum kept the bands linked to chitosan, with a broad band near 3447 cm-1 from the amino and hydroxyl groups and a band near 1639 cm-1 from the amide region, and no unexpected peaks appeared. The trend confirms that there is no chemical reaction taking place in the process but entrapment of the drug in the matrix, consistent with findings on metformin-chitosan systems in previous studies whereby FTIR analysis had revealed compatibility following encapsulation (Awchee *et al*., 2026).

Microscopy indicated that the particles were mainly spherical with moderate uniformity in shape with a mean size of around 200 nm. DLS resulted in a mean size of approximately 213 nm with a very low polydispersity index of less than 0.30, indicating particles of similar size with mean zeta potential of +28.1 mV. This positive charge allows for prevention of aggregation and facilitates binding to the negative surface of the cell membrane/mucus. These sizes of particles have a higher probability of uptake into cells compared to large microparticles and can remain in the gastrointestinal tract for longer periods (Salatin *et al*., 2015). There was some tendency for clumping when the suspension had been stored for some time; hence, the surface charge provides some degree of protection against clumping but not enough during the storing period. The entrapment efficiency of the particles was 97.34%. The drug was released from the particles steadily over 24 hours, thus being completely released by this point in time. The steady release of this nature allows maintaining the level of the drug stable and not allowing any peaks.

Administration of MTX in Group B resulted in changes in the blood parameters characteristic of bone marrow suppressing drugs. There was a reduction in red blood cell count, hemoglobin content, hematocrit index, total leukocyte count, lymphocyte percentage, and platelet count and increase in neutrophil and monocyte percentages and mean cell hemoglobin. In particular, red blood cell count decreased from 8.10 to 3.67 x10^12/L, hemoglobin content – from 15.4 to 9.8 g/dL, and platelets – from 980 to 430 x10^9/L. These changes are characteristic of MTX, which inhibits DNA synthesis in proliferating cells in a folate-dependent way and induces systemic inflammation due to oxidative stress and cytokines release (Genestier *et al*., 2000; Howard *et al*., 2016). Combined, they indicate that chronic MTX administration leads to disruptions in the process of erythropoiesis as well as the ratio of immune cells.

The correction of these parameters occurred in a dose-dependent manner; Group H (75 mg/kg/day) demonstrated the highest effectiveness in comparison with other treatment groups. The red blood cell number, hemoglobin and hematocrit values increased gradually with increasing nanoparticle concentration up to their approaching the value of the healthy control and blank nanoparticle group. In the same way, the platelet count increased

gradually from 470 to 650 to 820x10^9/L in the low, middle and high nanoparticle concentrations, respectively. The increase in the number of red cells and platelets implies restoration of bone marrow function, and the shift of white cell distribution towards normally indicates the reduction of systemic inflammation. It is known that metformin reduces inflammatory signaling via activation of AMP-activated protein kinase (AMPK) which results in suppression of NF-kappa activity and inflammatory mediators (Kristófi and Eriksson, 2021). Group E with free metformin was the least effective of the active groups for blood parameters, and neither Group E nor Group C were significantly differentiated from the toxic control concerning the total leukocyte count. However, the reference drug silymarin had contradictory effects; it successfully normalized the total leukocyte count, yet increased the percentage of neutrophils above the toxic control and failed to normalize the percentage of lymphocytes, which were normalized in Groups D and C. The increased efficacy and consistency of nanoparticles can be explained through the activity of metformin and the continuous supply of the drug by the chitosan nanocarrier (Awchee *et al*., 2026).

The results of serum chemistry in Group B revealed that MTX caused the damage to the liver. There was an increase in AST, ALT, ALP, and total bilirubin concentrations and a decrease in total protein and albumin levels. AST was 312.5 U/L compared to 82.0 in the healthy control, ALT – 190.0 compared to 44.0, ALP – 582.59 compared to 155.0, and total bilirubin – 7.61 mg/dL compared to 0.42 Increase in transaminases indicates hepatocyte membrane injury and the release of enzymes into the bloodstream, whereas an increase in bilirubin suggests the impairment in bile secretion. A decrease in albumin and total proteins indicates poor protein synthesis due to prolonged exposure to MTX. Changes observed in these parameters are consistent with previous observations that link MTX-induced liver injury to oxidative stress, mitochondrial dysfunction, and inflammatory infiltration (Howard *et al*., 2016).

Active treatments significantly decreased elevated parameters and increased reduced parameters compared to the control group with toxicity. Dose-dependent effects were also seen in the treatment with nanoparticles. Free metformin (Group E) once again produced the least amount of improvement: AST = 178.0, ALT = 95.0, ALP = 360.0, and bilirubin = 2.85 mg/dL. Groups with nanoparticles showed dose-dependent improvements, and the high-dose group (Group H) had values that were most similar to those of the healthy control: ALT = 40.5 U/L (almost equal to the value in the control group: 44.0) and bilirubin = 0.95 mg/dL. Albumin and total proteins showed similar results with the values in Group H being 6.6 and 3.8 g/dL respectively. The blank-particle group was comparable to the healthy control group in terms of all biochemistry parameters, and this suggests that the carrier itself had no detrimental effects on the liver. The enhanced effectiveness of the nanoparticle formulation relative to free metformin is in keeping with the theory that the chitosan formulation enhances the efficacy of the drug. Silymarin provided a valuable point of comparison in light of its protective action against damage to the liver (Vargas-Mendoza *et al*., 2014).

The histological results were consistent with the biochemical findings. The sections of the livers from the MTX group displayed widespread hepatocytes degeneration, dilation of the sinusoids, dense inflammatory infiltrate, necrotic areas, and abnormality of the hepatic lobules structure. This group had median activity score of 6 and median fibrosis stage of 4, with most of the rats developing advanced fibrosis. All of these characteristics are common for MTX-induced liver injury. One possible pathway is through prolonged oxidative stress during MTX metabolism, followed by lipid peroxidation, mitochondrial dysfunction, migration of inflammatory cells, and activation of hepatic stellate cells. The degree of injury confirms that there was genuine hepatotoxicity and it is responsible for serum alterations observed previously.

Metformin and silymarin had incomplete protective effect, since they reduced the median value of the activity score to 3 and the stage of fibrosis to 3, but none of them was statistically significant versus toxic control in respect to necro-inflammation, and none reduced fibrosis. Nanoparticles showed better results. Low and medium doses reduced the median value of the activity score to 1, the stage of fibrosis to 2, and both indicators were statistically significantly lower than those in the toxic control in respect to necro-inflammation. The high dose of nanoparticles (Group H) had the best results, characterized by neat organization of hepatic cords, lack of sinusoidal congestion, low numbers of inflammatory cells, rare necrotic areas, activity score of 0 in the majority of rats and no fibrosis at all. Among all experimental groups, the only one, 75 mg/kg/day nanoparticles, reduced fibrosis significantly versus MTX. Thus, the antifibrotic effect is related only to high dose of nanoparticles.

Considering the molecular aspect of this protection, we studied the expression of *TGF-β* and *TIMP1*, the two most important genes responsible for fibrosis of the liver. *TGF-β* is the key profibrotic molecule that stimulates hepatic stellate cells to transform into myofibroblasts producing collagen. The role of *TIMP1* is the inhibition of matrix metalloproteinases; thus, it results in the slow degradation of the extracellular matrix and formation of the fibrotic tissue. MTX induced the expression of the two genes in toxic control, namely, 6.77 times in case of *TIMP1* and 4.66 times in case of *TGF-β*.

It is interesting that the two genes behaved differently. For *TIMP1*, every treatment brought expression below the toxic-control level. Silymarin gave the lowest value (0.62-fold), followed by the high and middle nanoparticle doses (1.74 and 1.87-fold) and the blank particles (1.93-fold), while the low nanoparticle dose (3.89-fold) and free metformin

(3.05-fold) were less effective. Across the three nanoparticle doses *TIMP1* fell steadily as the dose rose, so the effect was dose-related, and the high dose gave the strongest suppression among the nanoparticle groups. For *TGF-β* the pattern was different. The high nanoparticle dose produced the largest drop of any group, to 0.51-fold, with silymarin and the blank particles also low, and the low and middle nanoparticle doses gave 3.05 and 1.57-fold, again a steady fall with rising dose. Free metformin, by contrast, raised *TGF-β* to 5.90-fold, above the toxic control itself, so the unpackaged drug failed to calm this signal and instead pushed it higher. The reason is not clear from the present data and may relate to the low oral bioavailability of free metformin and to dose- and context-dependent effects on *TGF-β* signaling, but the packaged form did not share this drawback. The drop in *TGF-β* and *TIMP1* in the nanoparticle groups tracked the lower fibrosis scores, which suggests that the change in gene expression carried through to the tissue. Metformin is known to limit *TGF-β* -driven fibrogenesis by activating AMPK and interfering with Smad-dependent transcription in hepatic stellate cells (Lim *et al*., 2012), and a lower *TIMP1* level would help restore the balance between matrix metalloproteinases and their inhibitors and reduce collagen build-up. This must be noted that although the blank-particle group had the same parameters of blood counts, serum biochemistry and histological structures, compared with the healthy control, the concentration of *TIMP1* in this group was somewhat higher (1.93-fold) than in the control, therefore the particle can hardly be referred to as completely non-functional molecule, since there was no adverse effect on function.

A number of limitations should be mentioned concerning this study. The pharmacokinetics study was not performed; hence, any assumption about the higher oral bioavailability and preference of accumulation of the drug in liver was made only based on inference. While gene expression was determined, the oxidative stress markers, inflammatory cytokines and protein assays were not evaluated, which does not allow fully studying the mechanism. The amplification efficiency was calculated based on the standard curve ($R^2 = 0.997$; slope −3.587; E ~ 0.90, ~90%), while normalization of the results was done using one reference gene (GAPDH); thus, the qPCR relative data should be considered supporting evidence. This experiment also involved the use of a rat model. Therefore, this information should be extrapolated to human disease with some level of care. In future studies, there is need for inclusion of pharmacokinetics, detailed investigation of oxidative and inflammatory pathway, tissue distribution studies, safety and toxicity tests for longer periods and in multiple preclinical models.

Conclusion: This study shows that metformin-loaded chitosan nanoparticles give real protection against MTX-induced liver injury in rats. The formulation improved blood counts, brought liver function markers back toward normal, kept liver structure intact, reduced fibrosis, and lowered the profibrotic genes *TGF-β* and *TIMP1*, with the 75 mg/kg/day dose giving the strongest and most consistent effect. Free metformin was the weakest active treatment and raised *TGF-β* above the toxic-control level, which shows that the benefit depended on the nanoparticle form rather than on metformin alone. The blank carrier caused no functional harm, although it produced a small rise in *TIMP1*. The match between the physical properties of the particles and the biological results suggests that nanoparticle delivery improved how well metformin worked in this model. With further pharmacokinetic and translational study, metformin-loaded chitosan nanoparticles look like a promising approach for lowering MTX-induced liver injury.

ACKNOWLEDGMENT: The authors are very grateful for their valuable guidance during the conduct of research.

Funding: None.

Data availability: All underlying data supporting the findings of this study will be available on request from corresponding author.

Conflict of Interest: The authors declare no conflict of interest.

Author Contributions: N.S., Conceptualization, Methodology and Writing-Original Draft. M.A.R., Supervision, Writing-Review and Editing. M.O.O. Data Curation, Formal Analysis and W.S. investigation and Visualization. All authors critically reviewed the manuscript and approved the final version.

REFERENCES

Al-Bhadly, O. and I.M. Mnati (2025). Chitosan nanoparticles as a therapeutic agent for mitigating paracetamol-induced liver damage in white male albino rats. Trop. J. Nat. Prod. Res. 9(9): 4137–4142. doi:10.26538/tjnpr/v9i9.9.

Awchee, Z.O., A.C. Ovenseri, A.S. Malkawi and L.B. Pozharani (2026). Formulation of metformin-loaded chitosan nanoparticles and in vivo evaluation of its hypoglycemic effects. Molecules 31(9): 1539. doi:10.3390/molecules31091539.

Bayda, S., M. Adeel, T. Tuccinardi, M. Cordani and F. Rizzolio (2019). The history of nanoscience and nanotechnology: From chemical-physical applications to nanomedicine. Molecules 25(1): 112. doi:10.3390/molecules25010112.

Bedoui, Y., X. Guillot, J. Sélambarom, P. Guiraud, C. Giry, M.C. Jaffar-Bandjee, *et al*. (2019). Methotrexate: An old drug with new tricks. Int. J. Mol. Sci. 20(20): 5023. doi:10.3390/ijms20205023.

Borah, P. (2011). Primer designing for PCR. Sci. Vis. 11(3): 134–136.

Brennan, P.N., P. Cartlidge, T. Manship and J.F. Dillon (2022). Guideline review: EASL clinical practice guidelines: Drug-induced liver injury (DILI). Frontline Gastroenterol. 13(4): 332–336. doi:10.1136/flgastro-2021-101886.

Chandor, S.B. (2006). Tietz textbook of clinical chemistry and molecular diagnostics. J. Am. Med. Assoc. 295(20): 2417–2418. doi:10.1001/jama.295.20.2417.

Ezhilarasan, D. (2021). Hepatotoxic potentials of methotrexate: Understanding the possible toxicological molecular mechanisms. Toxicology 458: 152840. doi:10.1016/j.tox.2021.152840.

Ezhilarasan, D., S. Karthikeyan, M. Najimi, P. Vijayalakshmi, G. Bhavani and M.J. Rani (2025). Preclinical liver toxicity models: Advantages, limitations and recommendations. Toxicology 511: 154020. doi:10.1016/j.tox.2024.154020.

Gardner, J. and A. Ghorpade (2003). Tissue inhibitor of metalloproteinase (TIMP)-1: The TIMPed balance of matrix metalloproteinases in the central nervous system. J. Neurosci. Res. 74(6): 801–806. doi:10.1002/jnr.10835.

Genestier, L., R. Paillot, L. Quemeneur, K. Izeradjene and J.P. Revillard (2000). Mechanisms of action of methotrexate. Immunopharmacology 47(2–3): 247–257. doi:10.1016/S0162-3109(00)00189-2.

Gornall, A.G., C.J. Bardawill and M.M. David (1949). Determination of serum proteins by means of the biuret reaction. J. Biol. Chem. 177(2): 751–766. doi:10.1016/S0021-9258(18)57021-6.

Guadarrama-Escobar, O.R., P. Serrano-Castañeda, E. Anguiano-Almazán, A. Vázquez-Durán, M.C. Peña-Juárez, R. Vera-Graziano, *et al*. (2023). Chitosan nanoparticles as oral drug carriers. Int. J. Mol. Sci. 24(5): 4289. doi:10.3390/ijms24054289.

Gujytė, G., G. Rapševičiūtė, A. Černiakova, I. Petrauskaitė, A. Liuizė and A. Mongirdienė (2026). Anti-inflammatory interleukins in the pathogenesis of atherosclerosis. Int. J. Mol. Sci. 27(11): 5030. doi:10.3390/ijms27115030.

Hafez, S.M.N.A. and E. Elbassuoni (2022). Dysfunction of aged liver of male albino rats and the effect of intermittent fasting: Biochemical, histological and immunohistochemical study. Int. Immunopharmacol. 103: 108465. doi:10.1016/j.intimp.2021.108465.

Howard, S.C., J. McCormick, C.H. Pui, R.K. Buddington and R.D. Harvey (2016). Preventing and managing toxicities of high-dose methotrexate. Oncologist 21(12): 1471–1482. doi:10.1634/theoncologist.2015-0164.

Kozielewicz, D.M., P. Stalke and J. Skrzypek (2025). Drug-induced liver injury. Part I: Classification, diagnosis and treatment. Clin. Exp. Hepatol. 11(1): 25–33. doi:10.5114/ceh.2025.148329.

Koźmiński, P., P.K. Halik, R. Chesori and E. Gniazdowska (2020). Overview of dual-acting drug methotrexate in different neurological diseases, autoimmune pathologies and cancers. Int. J. Mol. Sci. 21(10): 3483. doi:10.3390/ijms21103483.

Kristófi, R. and J.W. Eriksson (2021). Metformin as an anti-inflammatory agent: A short review. J. Endocrinol. 251(2): R11–R22. doi:10.1530/JOE-21-0194.

Kube, D.M., C.D. Savci-Heijink, A.F. Lamblin, F. Kosari, G. Vasmatzis, J.C. Cheville, D.P. Connelly and G.G. Klee (2007). Optimization of laser capture microdissection and RNA amplification for gene expression profiling of prostate cancer. BMC Mol. Biol. 8: 25. doi:10.1186/1471-2199-8-25.

Lim, J.Y., M.A. Oh, W.H. Kim, H.Y. Sohn and S.I. Park (2012). AMP-activated protein kinase inhibits *TGF-β* -induced fibrogenic responses of hepatic stellate cells by targeting transcriptional coactivator p300. J. Cell. Physiol. 227(3): 1081–1089. doi:10.1002/jcp.22824.

Livak, K.J. and T.D. Schmittgen (2001). Analysis of relative gene expression data using real-time quantitative PCR and the 2−ΔΔCT method. Methods 25(4): 402–408. doi:10.1006/meth.2001.1262.

Mast, M.P., H. Modh, J. Knoll, E. Fecioru and M.G. Wacker (2021). An update to dialysis-based drug release testing: Data analysis and validation using the Pharma Test Dispersion Releaser. Pharmaceutics 13(12): 2007. doi:10.3390/pharmaceutics13122007.

Mathane, A.M., P.R. Hatwar and R.L. Bakal (2025). Biodegradable polymer use in drug delivery systems: A comprehensive review. J. Drug Deliv. Ther. 15(10): 201–211. doi:10.22270/jddt. v15i10.7421.

Meng, X.M., D.J. Nikolic-Paterson and H.Y. Lan (2016). TGF-β: The master regulator of fibrosis. Nat. Rev. Nephrol. 12(6): 325–338. doi:10.1038/nrneph.2016.48.

Mishra, P., C.M. Pandey, U. Singh, A. Gupta, C. Sahu and A. Keshri (2019). Descriptive statistics and normality tests for statistical data. Ann. Card. Anaesth. 22(1): 67–72. doi: 10.4103/aca.ACA_157_18.

Mohamadnejad, M., S.M. Tavangar, M. Sotoudeh, F. Kosari, M. Khosravi, B. Geramizadeh, *et al*. (2010). Histopathological study of chronic hepatitis B: A comparative study of Ishak and METAVIR scoring systems. Int. J. Organ Transplant. Med. 1(4): 171–176.

Naqvi, I.H., K. Mahmood, A. Talib, A. Mahmood, I. Naqvi and K. Mahmood (2015). Antituberculosis drug-induced liver injury: An ignored fact, assessment of frequency, patterns, severity and risk factors. Open J. Gastroenterol. 5(12): 173–184. doi:10.4236/ojgas.2015.512027.

Naskar, S., K. Koutsu and S. Sharma (2019). Chitosan-based nanoparticles as drug delivery systems: A review on two decades of research. J. Drug Target. 27(4): 379–393. doi:10.1080/1061186X.2018.1512112.

Ozturk, N.B., E. Uskudar, M.D. Toruner, C. Simsek and A. Gurakar (2024). Drug-induced liver injury: Diagnosis, management and the role of liver transplantation. Hepatol. Forum 6(2): 72–76. doi:10.14744/hf.2024.2024.0003.

Pivovarov, K. and J.S. Zipursky (2019). Low-dose methotrexate toxicity. CMAJ 191(15): E423. doi:10.1503/cmaj.181054.

Rani, S., C. Sharma, D. Jain, P. Chaudhary and D. Bhatia (2025). Urtica dioica L. attenuates methotrexate-induced hepatotoxicity in rats. Lett. Appl. NanoBioSci. 14(2): 71. doi:10.33263/LIANBS142.071.

Rio, D.C., M. Ares Jr., G.J. Hannon and T.W. Nilsen (2010). Purification of RNA using TRIzol (TRI reagent). Cold Spring Harb. Protoc. 2010(6): pdb.prot 5439. doi: 10.1101/pdb.prot 5439.

Rojas, L.B.A. and M.B. Gomes (2013). Metformin: An old but still the best treatment for type 2 diabetes. Diabetol. Metab. Syndr. 5(1): 6. doi:10.1186/1758-5996-5-6.

Salatin, S., S. Maleki Dizaj and A. Yari Khosroushahi (2015). Effect of the surface modification, size, and shape on cellular uptake of nanoparticles. Cell Biol. Int. 39(8): 881–890. doi:10.1002/cbin.10459.

Santhosh Kumar, C., D. Karthikeyan and V.R. Gadela (2017). Enhanced effects of metformin-loaded chitosan nanoparticles in L6 myotubes: In vitro. Der Pharmacia Lettre. 9(7): 48–63.

Singh, M., V. Sharma, A. Shrivastav, P. Singh and N. Verma (2023). Nanotechnology for novel drug delivery: A systematic review of classification, preparation, characterization, and applications of nanoparticles in drug delivery. Biosci. Biotechnol. Res. Asia 20(4): 1147–1165. doi:10.13005/bbra/3165.

Vargas-Mendoza, N., E. Madrigal-Santillán, Á. Morales-González, J. Esquivel-Soto, C. Esquivel-Chirino, M.G. García-Luna y González-Rubio, *et al*. (2014). Hepatoprotective effect of silymarin. World J. Hepatol. 6(3): 144–149. doi:10.4254/wjh. V 6.i3.144.

Zhang, J., Q. Liu, J. He and Y. Li (2021). Novel therapeutic targets in liver fibrosis. Front. Mol. Biosci. 8: 766855. doi:10.3389/fmolb.2021.766855.